03

Enhancement of the method of A.N. Ivanov for flows with free boundaries (to the 100th anniversary of Ivanov's birth)

© E.L. Amromin

Federal Way WA
98003, USA
e-mail: amromin@aol.com

Received August 31, 2022
Revised October 10, 2022
Accepted October 10, 2022

The analysis of flows with free boundaries is a non-linear problem, since their forms are not known in advance and must be found. The described method is effective for various problems with various dynamic conditions on free boundaries. This iterative method is based on the quasi-linearization of the boundary conditions for the velocity potential proposed by A.N. Ivanov in 1962. The iterations include the successive solutions of the Fredholm integral equations of the second kind (allowing to determine the pressure over a known boundary) and singular integral equations (to correct the boundary shape). Here both the general formulation of the method and its development for specific types of flows are presented, as well as numerous examples of solutions for them.

Keywords: cavitation, waves, quasi-linearization, iterations.

DOI: 10.21883/TP.2023.01.55439.212-22

Introduction

The goal of this work is to summarize the achievements obtained on the basis of the method proposed by professor A.N. Ivanov (1923–2006) for flows with free boundaries — cavitation and Stokes waves. Later, this method was developed for a wider variety of problems: wing stall, capillary waves, etc. However, all modifications keep the similarity with the original. It is worth to summarize them, and the jubilee of A.N. Ivanov, an alumnus of the Loytsyansky department in the Leningrad Polytechnic Institute (now the Peter the Great St.Petersburg Polytechnic University), who worked for more than half a century in the A.N. Krylov State Research Center, is a good reason for it.

The analysis of flows with free boundaries is a non-linear problem, since their forms are not known in advance and must be found on the basis of dynamic conditions. The Kirchhoff solution for two-dimensional flow downstream of a flat plate published in 1869 was the first solution to this problem. More than a century after it main methods of analysis of such problems were based on the variables inversion. We remind its basis using the Riabouchinsky's modification of the Kirchhoff problem. This modification (which is described, in particular, in [1]) allowed investigating the constant pressure zones with limited lengths. A fictitious boundary/body beyond such zone was introduced [2] to avoid the d'Alembert paradox. In the ideal fluid theory, fluid velocity U at the boundary of this zone is constant, but it increases gradually from zero to U_0 along an obstacle and decreases gradually along the fictitious boundary. Therefore, the image of flow boundary downstream of a flat plate or a disc in the plane of transformed variables $\{U, N_X\}$, where N — normal to the partly unknown boundary S, is just a rectangle. The inversion of the unknown part S in the $\{x,y\}$ space into a line segment in this plane often simplifies the calculations for plane problems, conformal mappings sometimes allow obtaining Exact solutions. Inversed variables were also used for axisymmetric cavitating flows downstream of obstacles of simple geometries [3].

However, an inversion of variables becomes useless for the analysis of flows over bodies with complex geometries. This is illustrated by the example of partial cavitation of the hydrofoil OK2003 shown in Fig. 1. Free boundary in the plane $\{x,y\}$ lays on the top side of the hydrofoil from its leading edge to the point with an abscissa of $x = 0.6C$, where C being its chord. Downstream of this point there is a fictitious body, value of U is unknown there. The image of the boundary of this flow in the plane $\{U, N_X\}$ is very complex and unknown are even the ends of the line segment $U = U_0$. The situation does not become better with the selection of another hodograph planes described in [4]: in general, the inversion of variables does not transform a partially unknown boundary into a fully known boundary in another planes.

Meanwhile, the linear theory [5] gives unsatisfactory results for profiles with significant variations of their curvature, such as sections of propeller blades. The pessimistic mood of the review in [6] regarding the situation with mathematical analysis of cavitation and its applicability to technical issues was understandable in 1971. Although the first breakthrough was already done by Ivanov [7,8] with the use of iteration methods in physical spaces $\{x,y\}$ and $\{x,y,z\}$, and another quasi-linear method was developed soon by Tulin [9], the influence of these innovations was not immediate. In the following decades two groups of iteration methods for cavitating flows of nonviscous fluid were developed. The first group uses modifications of the

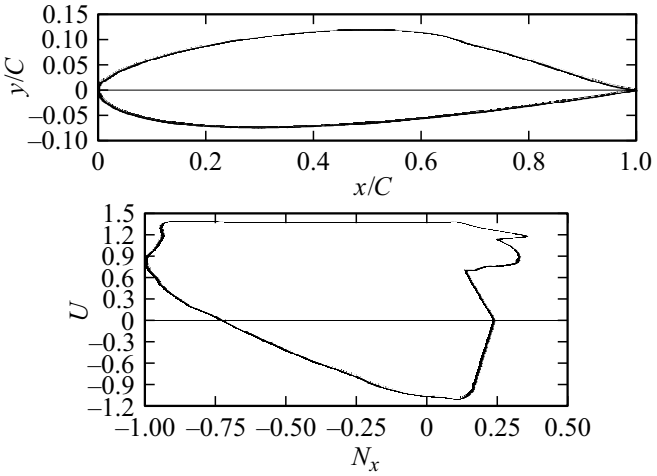

Figure 1. Boundaries of flow over the cavitating Hydrofoil OK2003 in $\{x, y\}$ and $\{U, N_x\}$ planes.

Ivanov's method in the exact non-linear formulation for plane and axisymmetric cavitating flows, starting from [10–14], and later [15–17] for more complicated problems. All iterations in all modifications of this method are composed of two parts. The first part — solving the Neumann problem. For velocity potential out of the approximately defined boundary S. The second part — correction of the boundary using a quasi-linearized dynamic boundary condition at the free boundary.

The second group of methods described in [18–23] uses iteration algorithms also based on solving two different problems in two successive parts of each iteration. The first problem is solved for the velocity potential with Neumann condition on known parts S and Dirichlet condition on the free surface. The second problem is a correction of S by integration of the kinematic boundary condition.

Since 2000 calculations of fully turbulent flows with variable density using RANS- or LES-codes often displace the calculations of nonviscous fluid flows with free boundary. The use of these codes (especially some commercial codes) can be referred to as a more simple normal approach. Nevertheless, according to experts [24,25], there are different problems where ideal fluid calculations yield better results. In addition, combinations of ideal fluid calculations and viscous flow calculations often can be useful, as in [26,27].

The description of initial version of the Ivanov's method and examples of its use were presented in the monograph [28] in addition to papers [7,8,29,30]. Later publications, where this method was also applied, did not include detailed descriptions of its modifications, being rather focused on the physics of the problems than on computation aspects of solving them. Nevertheless, the successful use of the same method for very different problems makes reasonable this description supported by new examples of solutions for them.

1. General formulation and quasi-linearization

Flows with free boundaries are considered here within the ideal fluid theory framework. A velocity potential is introduced that meets the Laplace equation

$$\Delta\Phi = 0 \tag{1}$$

and the boundary condition for its normal derivative on S:

$$\frac{\partial\Phi}{\partial N} = F_1 \tag{2}$$

with a set function F_1. Also, the inflow is set, for example

$$\left.\frac{\partial\Phi}{\partial x}\right|_{x\to-\infty} = 1. \tag{3}$$

The potential and its derivatives here are normalized using inflow velocity U_∞ and size of the body. With fixed S equations (1)−(3) describe the Neumann problem. It is stated in the course of mathematical physics [31], that for regions outside the closed limited surface S this linear problem has a single solution. However, there is also a dynamic condition, which is a consequence of the momentum equation integral on the part of S that belongs to the free surface S_F:

$$\frac{\partial\Phi}{\partial s} = F_2, \tag{4}$$

where F_2 is a function that can be dependent on coordinates S_F, their derivatives or on derivatives of Φ. This condition makes impossible solving the problem (1)−(4) out of an arbitrarily-shaped boundary. Therefore, the shape of S_F here is unknown initially, and conditions (2), (4) are non-linear for any F_1, F_2, and all the problem is non-linear. For different right parts of equations (2), (4) in various physical problems the algorithm of their solving by the method is mainly the same. At any iteration first it is necessary to find $U = \mathrm{grad}(\Phi)$ on S by solving equations (1)−(3) with the shape of S obtained at the previous iteration; the initial shape should be defined before the first iteration. This solution can be found by different numerical methods. In particular, the author has used boundary element methods. The resulted distribution of U over S needs to be substituted in equation (4). The iterations are stopped and S is adopted as the final boundary of the flow when the difference between left and right parts of equation (4) nowhere exceeds a set small value. Otherwise a quasi-linear inverse problem has to be solved and S_F has to be corrected before the next iteration.

The correction of S can be interpreted as a motion opposite to the gradient in the auxiliary system of variables that define the shape of S_F. Though an analytical description of this surface might exist sometimes, the general approach is its stepwise determination using M points distributed over

this surface. Let us start from the two dimensional case and denote coordinates of these points as

$$x_m^{k+1} = x_m^k + h_m^k N_{xm}^k, \qquad y_m^{k+1} = y_m^k + h_m^k N_{ym}^k, \quad (5)$$

where superscripts indicate iteration numbers, and subscripts are numbers of points. Quasi-linearization of equations (2), (4) allows determining components of the antigradient $\mathbf{h^k}$ on S_F^k. This quasi-linearization in the point $\{x_m^{k+1}, y_m^{k+1}\}$ will be implemented using a solution to equations (1)–(3) in the point $\{x_m^k, y_m^k\}$. Normal and tangent lines to S_F^k are denoted as n and τ. Normal and tangent lines to S_F^{k+1} are N and T. The difference of velocity components in nearly points $\{x_m^{k+1}, y_m^{k+1}\}$ and $\{x_m^k, y_m^k\}$ is caused, first by the small rotation of the normal, second by the short distance h between these points, third by the small change Φ of potential between them due to the small perturbance q. Here

$$\varphi(q, S_F^k) = \begin{cases} \frac{1}{2\pi}\int q \ln|r| ds & -2D\ case, \\ \frac{1}{4\pi}\iint \frac{q}{r} ds & -3D\ case, \end{cases} \quad (6)$$

$\{x, y, z\}$ — coordinates of the point where the potential is calculated, and points with coordinates $\tilde{x}, \tilde{y}, \tilde{z}$ located on S_F^k. In the two-dimensional case $r = \sqrt{(x-\tilde{x})^2 + (y-\tilde{y})^2}$, in the three-dimensional case $r = \sqrt{(x-\tilde{x})^2 + (y-\tilde{y}^2 + (z-\tilde{z})^2}$. In the left part of equation (3) the derivative

$$\frac{\partial \Phi}{\partial N} = \frac{\partial \Phi}{\partial n}\cos(N, n) + \frac{\partial \Phi}{\partial \tau}\cos(N, \tau) \quad (7)$$

over S_F^{k+1} can be rewritten as follows:

$$\left.\frac{\partial \Phi}{\partial N}\right|_{S_F^{k+1}} = \left.\frac{\partial \Phi}{\partial n}\right|_{S_F^{k+1}} - \left.\frac{\partial \Phi}{\partial \tau}\right|_{S_F^{k+1}} \frac{\partial h}{\partial \tau}, \quad (8)$$

using the connection between the derivative h and small rotation of the normal. Replacement of the decomposition

$$\left.\frac{\partial \Phi}{\partial n}\right|_{S_F^{k+1}} = \left.\frac{\partial \Phi}{\partial n}\right|_{S_F^k} + \left.\frac{\partial \varphi}{\partial n}\right|_{S_F^k} + h\left.\frac{\partial^2 \Phi}{\partial n^2}\right|_{S_F^k}, \quad (9)$$

in (8) fallowed by the consideration of equation (2) at both boundaries results in the following equation:

$$\left.\frac{\partial \varphi}{\partial n}\right|_{S_F^{k+1}} + \left.\frac{\partial (Uh)}{\partial \tau}\right|_{S_F^k} = F_1(S_F^k) - F_1(S_F^{k+1}), \quad (10)$$

that establishes a relation between h and q. This equation is linear. By transforming the left part of equation (4) in the similar way, we get:

$$\frac{\partial \Phi}{\partial T} = \frac{\partial \Phi}{\partial n}\cos(T, n) + \frac{\partial \Phi}{\partial \tau}\cos(T, \tau), \quad (11)$$

$$\left.\frac{\partial \Phi}{\partial T}\right|_{S_F^{k+1}} = \left.\frac{\partial \Phi}{\partial \tau}\right|_{S_F^{k+1}} - \left.\frac{\partial \Phi}{\partial n}\right|_{S_F^{k+1}} \frac{\partial h}{\partial \tau}, \quad (12)$$

$$\left.\frac{\partial \Phi}{\partial \tau}\right|_{S_F^{k+1}} = \left.\frac{\partial \Phi}{\partial \tau}\right|_{S_F^k} + \left.\frac{\partial \varphi}{\partial \tau}\right|_{S_F^k} + h\left.\frac{\partial^2 \Phi}{\partial \tau \partial n}\right|_{S_F^k}. \quad (13)$$

However, in the right part of quasi-linearized equation (4) the curvature ϑ arises

$$F_2\left(S_F^{k+1}\right) = F_2\left(S_F^k\right) - F_1\left(S_F^{k+1}\right)\frac{dh}{d\tau} + \left.\frac{\partial \varphi}{\partial \tau}\right|_{S_F^k} - hU\vartheta|_{S_F^k}. \quad (14)$$

The derivation for the replacement of $\frac{\partial^2 \Phi}{\partial \tau \partial n}$ with ϑ is rather cumbersome and omitted here. Thus, it is possible to determine h_m^k and then to use of equation (5) to correct S_F^k after the difference between the set right part of equation (4) and its value on S_F^k is determined.

Usually, in time-independent problems with free boundaries, $F_1 = 0$. Then

$$\left.\frac{\partial \varphi}{\partial n}\right|_{S_F^k} + \left.\frac{(Uh)}{\partial \tau}\right|_{S_F^k} = 0, \quad (15)$$

$$\left.\frac{\partial \varphi}{\partial \tau}\right|_{S_F^k} - hU\vartheta|_{S_F^k} = F_2\left(S_F^k\right) - U. \quad (16)$$

It is important to note that equation (16) is a singular integral equation in q, while the calculations of $F_2\left(S_F^k\right)$ usually are based on the solution to integral Fredholm equations of the second kind. To integrate equations of different kinds, different grids are preferable, therefore interpolations of U, h, and q from one grid to another are needed.

This general description needs to be supplemented by specific recipes for the most effective solving of different types of problems. These recipes will be illustrated by computational examples in the following sections of this work.

2. Problems with constant right part of the dynamic condition

The oldest problems for flows with free boundaries correspond to $F_1 = 0$ and $F_2 = \sqrt{1+\sigma}$. Here $\sigma = 2(P_\infty - P_{\text{cavity}})/(\rho U_\infty^2)$ — cavitation number. These problems describe flows, where σ is a constant value. This type of F_2 corresponds to the condition of constant pressure with negligible gravity-to-inertia ratio on a free surface. Typical scheme of these two-dimensional problems is shown in Fig. 2.

Here, the flow boundary is composed of three parts. The first part is wetted surface of the hydrofoil. This parts remains unchanged in the process of iterations. The second part is free surface (the surface of the cavity). Its shape needs to be found in the process of iterations. The third parts encompasses the rear part of the cavity, where the real flow is extremely unstable, and yielding both equation (2) and equation (4) is impossible in this part. As it is described in the monograph [32], different schemes have been proposed for this area. In particular, here we use of

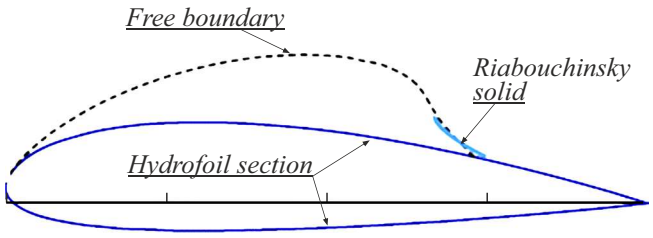

Figure 2. Scheme of two-dimensional cavitating flow over a hydrofoil. Dashed curve — free boundary.

the Riabouchinsky's solid, which length is fixed, while its vertical dimension varies from iteration to iteration.

For the $\{F_1, F_2\}$ under consideration in section 2, equation (16) can be further simplified. It becomes allowable to neglect the third term in the right part of equation (16) along the main part of the free surface (except for a fairly small neighborhood of its edges), because it has low curvature there. In the same part and due to the same reason the second term in the right part of equation (16) can be simplified to a Cauchy integral. As a result, this equation can be rewritten as follows:

$$U + \frac{1}{2\pi}\int\limits_{s_0}^{s_1} \frac{q(\tilde{s})}{s-\tilde{s}}d\tilde{s} = \sqrt{1+\sigma}. \qquad (17)$$

Then an inversion of the Cauchy integral can be applied to equation (17)

$$q = -2\frac{Z(s)}{\pi}\int\limits_{s_0}^{s_1} \frac{\sqrt{1+\sigma}-U}{Z(\tilde{s})(s-\tilde{s})}d\tilde{s}. \qquad (18)$$

As it is described in [33], there are four types of infersion. Three of them

$$Z(s) = \begin{cases} Z_0^0 \equiv \sqrt{(s-s_0)(s_1-s)}, \\ Z_0^\infty \equiv \sqrt{(s-s_0)/(s_1-s)}, \\ Z_\infty^0 \equiv \sqrt{(s_1-s)/(s-s_0)}, \end{cases} \qquad (19)$$

are engaged in the problem under consideration.

The same assumption regarding the curvature of the free surface allows simplification of equation (15) to $\frac{q}{2} = \frac{d(Uh)}{d\tau}$. However, if we substitute this formula directly in equation (18), it would impair the iteration convergence, because velocity along S has the number of continuous derivatives one fewer than that of its coordinates. Therefore, a certain smoothing is required before corrections of S_F, and first the value of q should be determined, and h should be found by integrating the following:

$$h(s) = \frac{b}{2U(s)}\int\limits_{s_0}^{s} q(\tau)d\tau + h(s_0). \qquad (20)$$

The corrected surface S must have continuous coordinates and components of normal. Two ways of such correction are possible for two-dimensional and axisymmetric flows. The first way corresponds to a fixed length of the cavity. The second way corresponds to a fixed value of σ. Different ways have different corresponding types inversion of Cauchy integral.

The algorithm of correction at a fixed value of σ is illustrated in Fig. 3. It is based on the use of two solutions to equations (18), (20) and their matching in the point x^*, where the least curvature of S_F takes place. The first solution uses Z_0^∞ and a fixed point s_0; based on this solution an abscissa x^* will be found; this solution defines the left branch of S_F. The second solution uses Z_0^∞ and a fixed point $s1$ in the equation for h, which is symmetric to equation (20); this solution defines the right branch of S_F and abscissa x^{**} with the same normal as in x^*, but x^{**} may differ from x^*. The branches are connected at $x = x^*$, however the right branch and the Riabouchinsky's solid will be moved over a distance of $x^{**} - x^*$ along axis x and over a distance of h^* along the perpendicular axis. This movement will be accompanied by a shift and a deformation of its contour with continuous coordinates and normal lines on its edges remained unchanged.

The correction algorithm for the cavity with a fixed length is based on solving equation (18) with $Z = Z_0^0$ and equation (20). In this case the additional condition of

$$\int\limits_{s_0}^{s_1} \frac{\left(\sqrt{1+\sigma}-U\right)d\tau}{Z_0^0(\tau)} = 0 \qquad (21)$$

should be met to make it possible the use of Z_0^0. This condition is also an equation to determine σ. Two branches of $h(x)$ are connected in a point with $N_X = 0$, and for the correction of S_F only vertical shift of the rear branch is needed.

As shown in Fig. 4, for the case of supercavitation, the same body can be considered as a cavitator and as a Riabouchinsky's body. The iteration process convergence is illustrated in Fig. 5 for an axisymmetric flow.

Fig. 6 shows distribution of the pressure coefficient over a cavitating hydrofoil after 80 iterations at $0.2 < b < 0.4$. Visible deviation of the calculated pressure coefficient from a constant value only remains near the leading edge of the cavity. The residual error in equation (4) at the edges of the cavity decreases much slower than that in the middle, because of the greater curvature of S_F near its edges; ϑ may even become infinite at the point s_0,and the last term in the

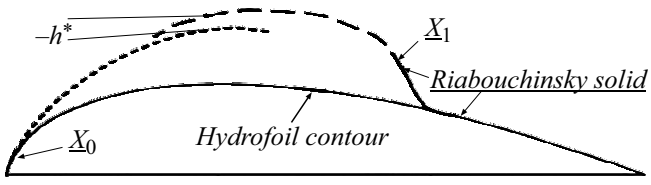

Figure 3. Scheme of cavity correction at a fixed σ.

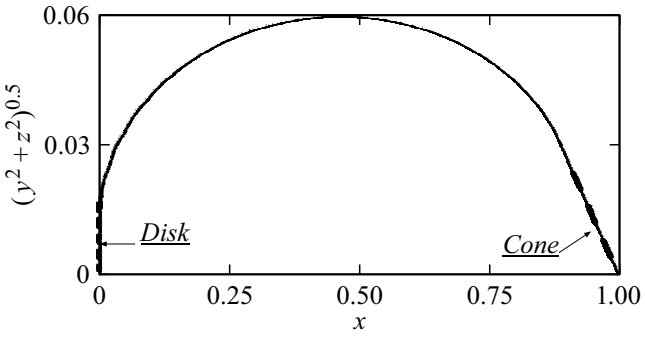

Figure 4. Meridional section of the cavity downstream of a disc with cone as a Riabouchinsky's solid (flow from the left) or the cavity downstream of a cone with disk as a Riabouchinsky's solid (flow from the right).

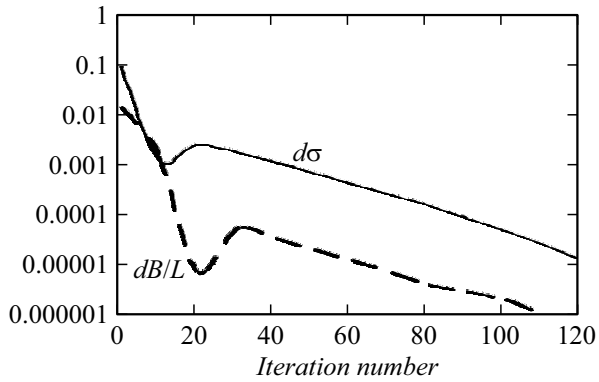

Figure 5. Convergence for the numerical solution of two-dimensional cavitating problems; $d\sigma$ — change in σ from iteration to iteration, dB — correspondent change in cavity thickness.

right part of (16) may not be negligible there. At the edges of S_F the asymptotic solution

$$h(s) = A_1(s - s_0)^{3/2} + \dots \qquad (22)$$

with uncertain coefficients A_1, A_2 was matched with the solution to equation (20).

In three-dimensional flows the cavity length is different along different streamlines. Meanwhile, tangent derivatives of Φ have the same feature there as the tangent derivatives in two-dimensional flows. Therefore, $3D$-equation (16) can be rewritten in the following form:

$$\frac{1}{2\pi}\int_{s_0}^{s_1}\frac{q(\tilde{s})}{s-\tilde{s}}d\tilde{s} = \sqrt{1+\sigma} - U - \frac{\partial\psi}{\partial\tau} \qquad (23)$$

using an auxiliary function without feature:

$$\psi(q,s) = \frac{1}{4\pi}\iint\frac{q}{r}ds - \frac{1}{2\pi}\int q\ln|r|ds. \qquad (24)$$

Equation (20) must be integrated along streamlines. The condition

$$\int_{s_0}^{s_1}\frac{\left(\sqrt{1+\sigma} - U - \frac{\partial\psi}{\partial\tau}\right)d\tau}{Z_0^0(\tau)} = 0 \qquad (25)$$

is written along streamlines as well, but in the three-dimensional case s_1 is an unknown parameter in equation (25), while σ is set and is the same for all streamlines.

A computational example of cavity Sections in a three-dimensional flow is shown in Fig. 7. We have used there a modification of Roshko's scheme with infinite cylinder downstream of the cavity instead of the Riabouchinsky's solid. As it was forecasted theoretically [1], Sections of the cavity downstream of a three-dimensional obstacle tend to circle.

A few general notes regarding the efficiency of calculations are relevant. First, as can be seen from Fig. 6, the solution to problem (1)–(3) at each iteration of the method used allows estimating how accurate is the solving

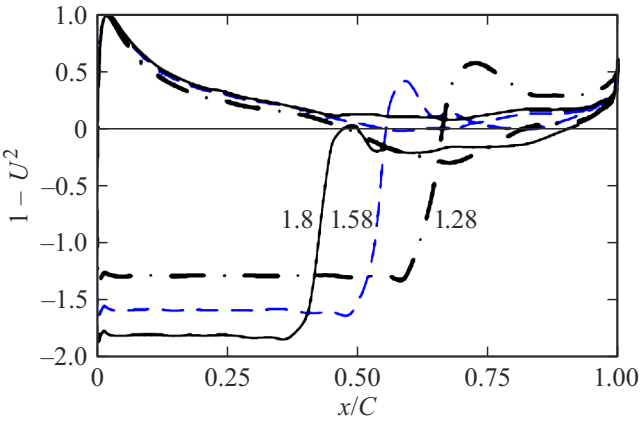

Figure 6. Measurement of dimensionless pressure coefficient $C_P = 1 - U^2$ around the hydrofoil ClarkY-11.7% with cavities at an attack angle of 8°; numbers near the curves identify correspondent values of σ.

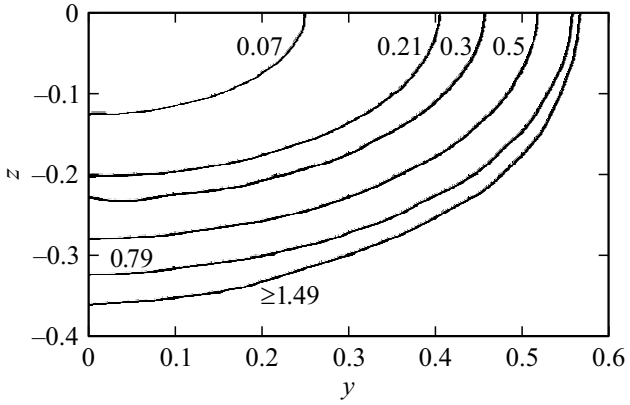

Figure 7. Sections of a three-dimensional cavity downstream of an elliptic obstacle at $\sigma = 0.2$. Numbers near the curves are values of coordinate x.

of both equation (2) and equation (4), and this is a significant advantage of the described method. Using the linear problem (1)−(3) in this way similar to the verification by the method of *manufactured solutions* of Roache [34]. In this case, for two-dimensional and axisymmetric flows there are well-known analytic solutions, which can be used to determine the required density of the grid. Then this density should be kept for more complex geometry of the body. Second, lower value of b should be used in equation (20) with decrease in σ. Third, the restriction imposed on the difference between left and right parts of equation (4) should be dependent on the accuracy of U calculation.

In addition to cavitating flows, there are also other problems where the right part of equation (4) is constant. One of these problems is related to plasma equilibrium figures [35]. The main role in such flow is played by mass forces, while the inertia force is negligible, but the calculation technique remains very similar.

3. Problems with coordinate-dependent dynamic conditions

As it was shown experimentally [36], the attached cavitation is a specific type of viscous separation. The pressure along separation zones is not constant, but increases significantly in their tail. Therefore the analysis of cavitation can be formulated more precisely as a problem with free boundary with a dynamic condition dependent on x, as it was suggested in [37]. The calculation of flows downstream of diaphragms in pipes is the simplest example of this type of problems. Scheme of this flow is shown in Fig. 8.

Pressure in such separation zone has a nearly isobaric part immediately downstream of the diaphragm, but increases at a certain distance upstream of the point of the boundary layer attachment to the pipe wall. The following equation:

$$\frac{1}{2\pi}\int_{s_0}^{s_1}\frac{qd\tilde{s}}{[s-\tilde{s}]} = C_0 + C_1 f_1(x) - U(x) - \frac{2U(x)h}{R} \quad (26)$$

is considered in this problem instead of equation (16). The first and the second terms in the right part of equation (26) reflect the change in pressure along the free surface. Along its isobaric part we have $f_1 = 0$, and downstream of it the pressure increases. The fourth term is an approximated

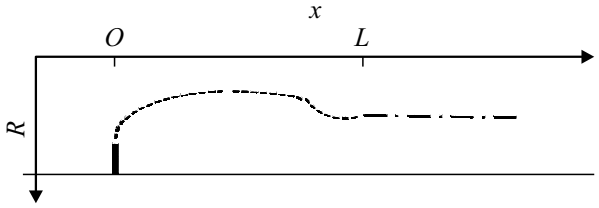

Figure 8. Scheme of the separation flow downstream of a diaphragm. The free surface is shown by dashed line, the fictitious body downstream of the separation zone is shown by dash-dotted line.

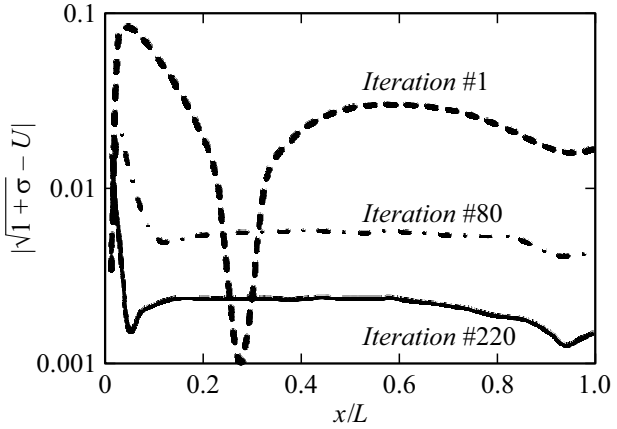

Figure 9. Example of the iteration process convergence in the problem of separation downstream of a diaphragm.

correction to U that takes into account the influence of change in the flow blocking between the pipe walls and S_F, caused by the correction of S_F.

For this inner flow problem (1)−(3) has no a single solution, and it must be replaced by the Dirichlet problem for current function. As a result U will be found by solving the following equation:

$$U + \frac{1}{2\pi}\frac{\partial}{\partial N}\iint U\frac{\cos\theta}{r}ds = -N_R\left(\frac{Q}{\pi R^2}\right), \quad (27)$$

where R is coordinate in a cylindrical coordinate system. Here, the current function is determined using vortices in axisymmetric flow.

With a set form of $f_1(x/L)$ in this problem there are three uncertain parameters: coefficients C_0, C_1, and L. To determine them, three conditions are required. The first of them is a generalization of equation (21) for the right part of equation (26). A simplified form of the momentum conservation law is

$$\frac{R(L)}{R(\infty)} = \left[\frac{1}{1+C_D}\right]^{\frac{1}{4}} \quad (28)$$

with an empirical value of the hole resistance coefficient (taken from the reference book [38]) is the second condition. The third condition is the criterion of boundary layer attachment $U = \xi RdU/dx$ at $x = L$, where ξ is an empirical coefficient. The iteration convergence for this problem is illustrated in Fig. 9. In this specific example, due to the significant flow blockage, a value of $b = 0.015$ was used (cross-section area of the hole is equal to 0.75 of the pipe cross-section).

As can be seen from Fig. 10, *a*, for other types of separating flows the function of F_2 can be more complex and include larger number of uncertain coefficients (as for the case of separation downstream of a backward facing step; comparison of calculations of [26] with measurements of [39,40] for this case is shown in Fig. 10, *b*). The additional coefficients require additional conditions dependent on the

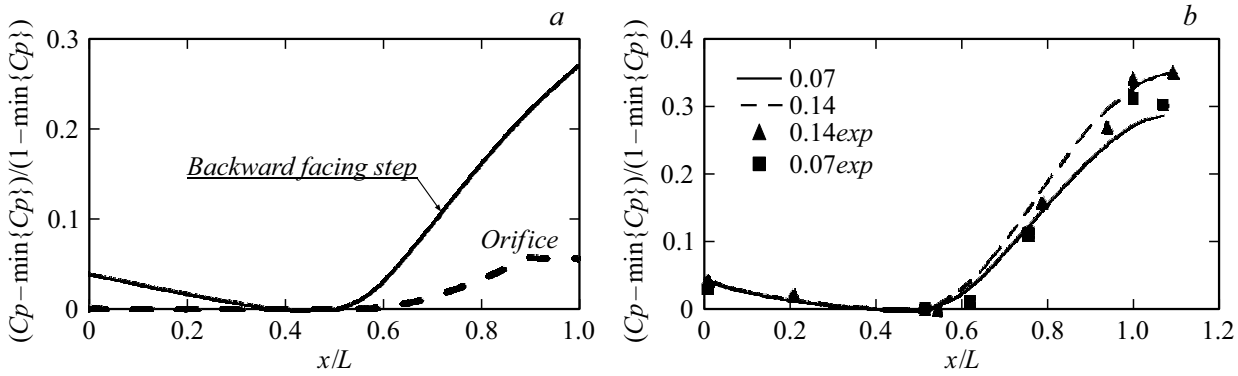

Figure 10. *a* — calculated normalized distributions of pressure along the separation zones downstream of various obstacles; *b* — comparison between calculated and measured pressure downstream of a step in a channel. Numbers indicate the ratio of the step height to the channel width.

version of the viscous-inviscid interaction procedure used. Its fundamentals are described in detail in [41,42], and since the description of these conditions is on no importance for the explanation of the method used, it can be omitted here.

The situation with the ordinate-dependent right part is similar to the previous situation from the mathematical point of view. It is interesting, that, as shown in [43], the fictitious body on the free surface can disappear due to ordinate-dependent mass forces as well.

The most important technical application of this effect is the ship drag reduction by ventilated cavitation, and the described method is used [44,45] for design of ship elements. In this case the cavity shape depends on more significantly, included in F_2, than on σ. This is shown in Fig. 11 taken from [44], where z_0 is an edge ordinate of the niche intended to stabilize the cavity under the ship bottom, $F_2 = \sqrt{1+\sigma} - 2(z - z_0)Fr^{-2}$, Froude number $Fr = U_\infty/\sqrt{gL}$, g — gravitational constant.

Another problem with this F_2 is the determination of non-linear gravitational waves. An example of its solving with the use of a generalization of the Ivanov's method is given in [46,47] for surface Stokes waves, which are non-linear waves with the critical point in the angles on their crests. Stokes waves are considered as stationary waves with maximum amplitudes [48]. The oldest solution [49] for Stokes waves was found for a flow with infinite depth. Later numerous solutions for surface Stokes waves were found by many authors, as a rule listed in the review of [50].

Inner waves are also often subjected to significant non-linear effects, as noted, in particular, in [51,52]. However, it is necessary to prove that inner Stokes wave can exist mathematically. Let us consider two infinite layers of ideal incompressible fluids with different densities, separated by the surface S. The Bernoulli equation for the top layer over S has the following form:

$$P + \rho_1 U_1^2/2\rho_1 gy = C_1, \tag{29}$$

and for the bottom layer it has the form of:

$$P + \rho_2 U_2^2/2 + \rho_2 gy = C_2. \tag{30}$$

Here ρ_1 and ρ_2 — densities of the first and the second fluids, U_1 and U_2 velocities in the first and the second fluids, y — ordinate of S. The pressure is continuous on the common current line of layers, thus $U_2^2 + 2gy - \varepsilon(U_1^2 + 2gy) = \frac{2(C_2 - C_1)}{\rho_2}$ there, where $\varepsilon = \frac{\rho_1}{\rho_2}$. Velocity of the ideal fluid on the angle edge can be either infinite, or zero. We use conform mappings to determine the zero-velocity angle. By considering an auxiliary half-plane $\{\xi\}$ for the bottom flow and using complex potential W there, we get $Z_2^\pi \sim \varsigma^\alpha$ and $U_2 \sim (dW/d\xi) \cdot \left(\frac{d\varsigma}{dZ_2}\right) \sim 1 \cdot Z_2^{\frac{\pi}{\alpha}-1}$, where $Z = x + iy$. A vicinity of the angle in the top flow can be mapped to the vicinity of the critical point on the circle. Therefore, $U_1 \sim \varsigma\, d\varsigma/dZ_1 \sim Z_1^{2\pi/(2\pi-\alpha)-1}$ and $Z_1^\pi \sim \varsigma^{2\pi-\alpha}$ there, but this mapping is only possible with a certain circulation of velocity related to vortices in the top flow. Since the sum of angles at the crest is 2π, the crest angle is $\alpha = 2\pi/3$, as for the surface Stokes waves.

Waveforms and intensities of related vortices are determined with the help of two Ivanov's contours shown in Fig. 12. The introduction of such contours, which geometry is known from previous iteration, allows replacement of the problem with infinite free surface by two connected problems with very large closed contour in an unlimited flow. This replacement simplifies the calculation to a significant extent. The initially unknown free surface is a relatively small common part of both contours. However, this part is much greater than the wavelength. Problem (1)−(3) for the contours can be solved using integral equations for the intensity of vortices distributed over them. This intensity is equal to the tangent velocity U in the bottom flow and $-U$ in the top flow, because there is no flow inside the contours. Different integral equations describe the bottom and the top flows. To derive them, we need to estimate the velocity induced on S by the vortices distributed over all other parts of the contour. Infinities of different orders must be analyzed. Let's assume that $|AH| = |AB| \ll |AE|$, $|CD| = |DG| \ll |FD|$, $|EF| \ll |AE|$,

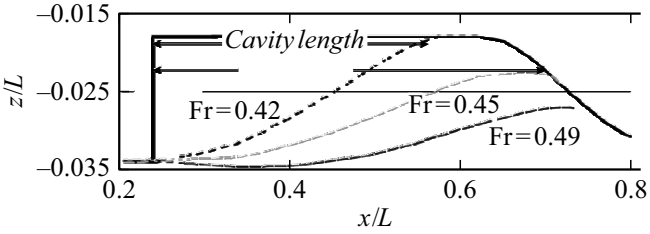

Figure 11. Influence of Froude number on two-dimensional cavities inside the niche. For this niche the height of the fictitious body 0 at Fr = 0.42 and 0.45, but $0.001 \cdot L$ at Fr = 0.49.

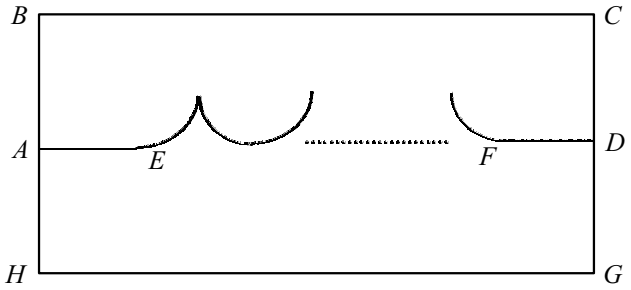

Figure 12. Scheme with Ivanov's contours AHGDFEA (in the top flow) and ABCDFEA (in the bottom flow).

$|EF| \ll |FD|$. For the top contour

$$\oint_{S^*} U\frac{\cos(N,R)}{R}dS = \int_E^F + \left(\int_F^D + \int_D^G + \int_H^G + \int_H^A + \int_A^E\right),$$

and

$$\oint_{S^{**}} U\frac{\cos(N,R)}{R}dS = \int_E^F + \left(\int_F^D + \int_D^C + \int_B^C + \int_A^B + \int_A^E\right)$$

— for the bottom contour. We can estimate the integrals over remoted parts of contours, taking into account that velocities along them are nearly unperturbed. Therefore, for the bottom flow we get:

$$U_2 - \frac{1}{\pi}\int_E^F U_2\frac{\cos(N,R)}{R}ds = N_Y V_1 + N_X V_2. \qquad (31)$$

Here

$$V_1 = \frac{1}{\pi}\left[a\tan\left(\frac{x-x_F}{y-y_A}\right) - a\tan\left(\frac{x-x_E}{y-y_A}\right)\right] - 1,$$

$$V_2 = \frac{1}{2}\ln\frac{(x-x_E)^2+(y-y_A)^2}{(x-x_F)^2+(y-y_A)^2}.$$

For the top flow it is necessary to take into account the induction of vortices, related to crests, and there we get:

$$U_1 + \frac{1}{\pi}\int_E^F U_1\frac{\cos(N,R)}{R}ds + \tilde{U} = (N_Y V_1 + N_X V_2)\beta, \quad (32)$$

β — ratio of inflow velocities in two flows, $\tilde{U} = \frac{\Gamma}{\pi}\sum_{k=-\infty}^{k=\infty}\frac{dX_k N_X + dY_k N_X}{dX_k^2+dY_k^2}$. The vortex intensity Γ is unknown, but the asymptotics $h(s) = \sqrt{s}(A_1 + A_2 s)$ is considered as an additional equation and can be used to determine this intensity. The position of the vortex system in the top part of flow is arbitrary and hence Γ depends on this position, like for vortices in the Tulin's scheme for the supercavitation [32]. Vortices in the presented calculations are located above the crests. In the nature, two layers of fluid with different densities moving at different velocities have a shear layer between them, and in this layer vorticity is created continuously, which is similar to the emergence of vorticity on a rigid flow boundary.

Quasi-linearized inverse problem is considered for one wave in the center of S. Prior to the next iteration, other waves will be copied from this wave. By assuming, that wave crests are located at a level of $y = 0$, we have $c_1 = c_2$. By assuming, that S is subjected to small perturbations only, we can simplify the constant pressure condition

$$2\varepsilon U_1 u_1 - 2U_2 u_2 - hN_Y\mu = F \qquad (33)$$

and introduce two auxiliary potentials of sources/sinks distributed along the selected wave on S; here u_1 and u_2 — perturbations of U_1 and U_2, $F = U_2^2 - \varepsilon U_1^2 + \mu y$, $\mu = 1 - \varepsilon$. Analogues of equation (20) in this problem are:

$$bq_1 = -2d(hU_1)/d\xi, \qquad bq_2 = \frac{2d(hU_2)}{d\xi}. \qquad (34)$$

Here q_1 and q_2 — presumably low intensities of perturbation potentials determined in two fluids. By substituting equation (34) into equation (32) and using inversion of Cauchy integral, we transform equation (34) into

$$\frac{\pi q_2}{Z_0^0(s)} - \int_\lambda\left[\frac{\varepsilon U_1}{\pi U_2}\int_\lambda\frac{d\left(\frac{U_1}{U_2}\int_0^\xi q_2 d\varsigma\right)}{d\xi}d\xi\right]\frac{dz}{\Pi}$$

$$-\int_\lambda\left[\frac{\mu N_Y}{U_2^2}\int_0^z q_2 d\varsigma\right]\frac{dz}{\Pi} = \int_\lambda\frac{F}{U_2}\frac{dz}{\Pi}. \qquad (35)$$

Here $\Pi = (s-z)Z_0^0(z)$. After solving equation (35), it is necessary to integrate the second equation (34) with respect to h with the initial condition of $h(0) = 0$ to the point of minimum $y + hN_Y$. This point is a wave trough on the corrected S. Then the right half-wave will be corrected symmetrically with respect to this point, and all the surface S will be covered with waves of the same shape. The determination of shape of periodic surface Stokes waves in infinite flow by the above-described method was considered as a verification of this method. Then it was reasonable to start calculations of inner Stokes waves from the options close to the verification example. The calculated waveforms for $\beta = 1$ and $\varepsilon \ll 1$ can be seen in Fig. 13 for

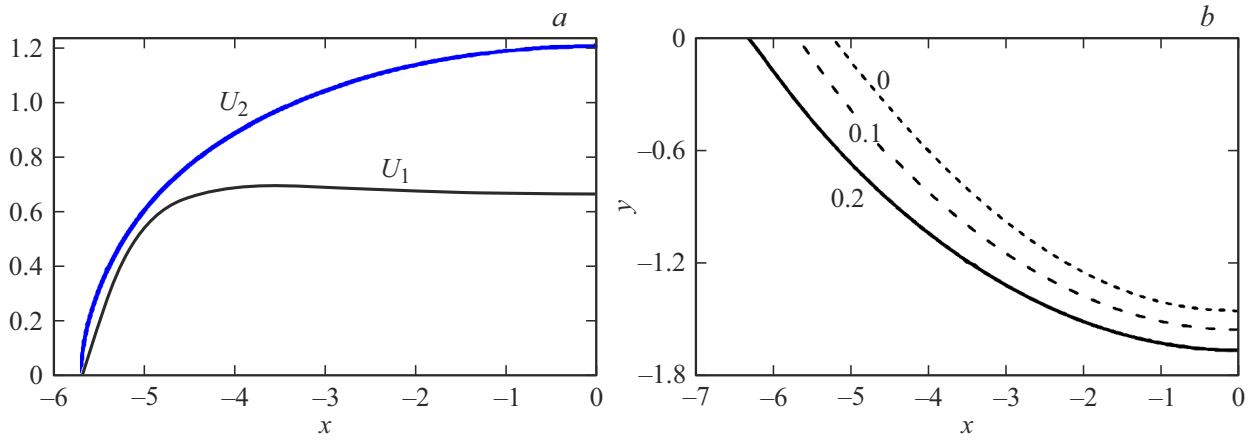

Figure 13. *a* — distribution of velocities in the top and bottom fluids along S for $\varepsilon = 0.1$, $\beta = 1$; *b* — waveforms for the values of ε indicated near the curves, $\beta = 1$.

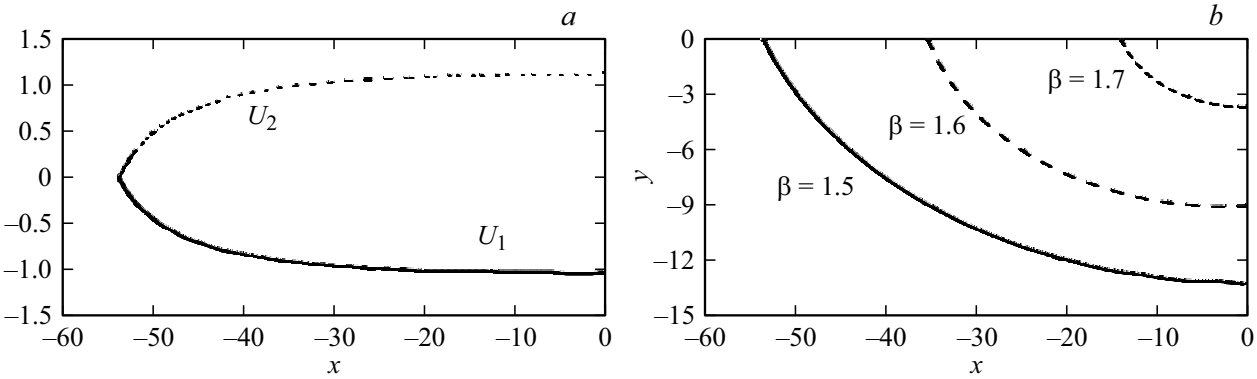

Figure 14. *a* — distribution of velocities in the top and bottom fluids along S for $\beta = -1.5$, $\varepsilon = 0.98$; *b* — waveforms of inner Stokes waves at different β and $\varepsilon = 0.98$.

different values of ε. Velocities in both fluids along their common boundary are compared in Fig. 13, *a* for $\varepsilon = 0.1$.

However, it is difficult to establish a relation between the examples with $\varepsilon = 0.1$ and 0.2 and well-observed flows. The observed flows with inner waves in the nature are referred to $\varepsilon \to 1$. The following examples of numerical solutions are referred to $\varepsilon = 0.98$, while the value of β is varied. In particular, the distributions of velocities in Fig. 14, *a* are referred to $\beta = -1.5$; thus, directions of flow in the top and bottom fluids in this example are opposite, as it took place in situations of mixing described in [53].

The ratio of height to wavelength for this wave is 0.1234, which is very close to the ratio of 0.141 for surface Stokes waves in an unlimited flow, but wavelength of the inner wave taken relative to $\Lambda = 0.5U_{1\infty}^2 g^{-1}$ is much higher. Wavelengths shown in Fig. 14 are dramatically dependent on β, but, as can be seen from Fig. 15, this does not lead to significant variations of wave slope or normalized intensities of vertices.

Equations (29), (30) will be satisfied with change of velocity sign. Therefore the above-presented results are true for $1.5 \le \beta \le 1.7$ and the same ε with the same $\Gamma/(\beta\lambda)$.

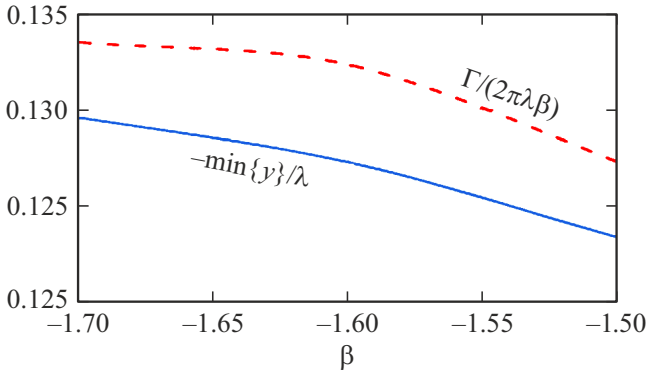

Figure 15. Dependencies of the Stokes wave slope (solid line) and normalized intensity of related vortices (dashed line) on β at $\varepsilon = 0.98$.

With $0.4 < \varepsilon < 0.8$ the numerical method used did not allow achievement of iteration convergence. Perhaps, Stokes waves simply do not exist with this ε.

4. Problems with boundary conditions dependent on the curvature

Finding capillary waves is a problem with a condition of the free boundary that depends on its curvature. The interest in this problem has grown in the last decades due to agiotage around the drag reduction with the use of hydrophobic coatings, and a lot of experimental studies have been performed in different ranges of Reynolds numbers (for example, described in [54–57]). The drag reduction occurs due to the air films adjoining these coatings. The modification of equation (4) for capillary waves on a film becomes $U^2 + 2\vartheta/We = 1 + \sigma$, where We — Weber number. The analogue of equation (16) in this problem is:

$$\frac{\widehat{k}}{We} + Uu + hU^2\vartheta = \frac{1+\sigma-U^2}{2} - \frac{\vartheta}{We}. \qquad (36)$$

Here $\widehat{k}$ — perturbation of ϑ. Despite the similarity of equation (36) with equation (17), the use of equation (20) derived from the latter is impossible in this problem. The matter is that the curvature of boundary has the number of continuous derivatives one fewer than that of u. Therefore, the unknown function $h(x)$ should be represented in the form of sum:

$$h = \sum_k A_k f_k(x) + \sum_k B_k g_k(x), \qquad (37)$$

where A_k and B_k — uncertain coefficients, and functions f_k, g_k meet the following conditions:

$$f_k\left(\frac{\lambda}{2}\right) = \frac{df_k}{dx}\left(\frac{\lambda}{2}\right) = \frac{dg_k}{dx}\left(\frac{\lambda}{2}\right) = \frac{df_k}{dx}(0) = \frac{dg_k}{dx}(0) = g_k(0) = 0. \qquad (38)$$

These coefficients are found by minimizing the right part of equation (36).

Examples of waveforms, calculated in [16] for capillary waves, are shown in Fig. 16. The approximations of h, similar to formula (37), were used in inverse problems as well [58–60], which also can be considered as problems with free boundaries.

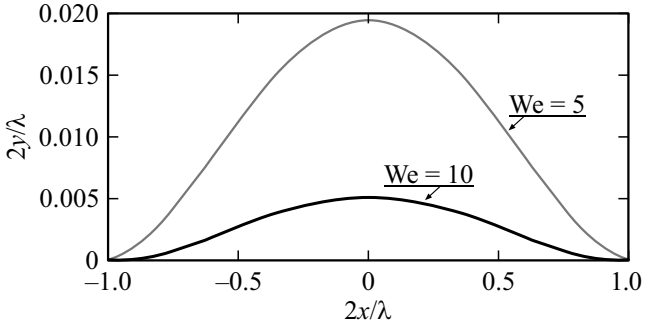

Figure 16. Calculated waveforms of capillary waves.

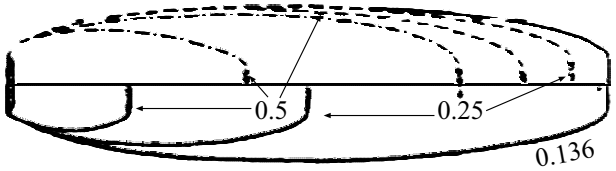

Figure 17. Meridional sections of axisymmetric cavities downstream of a disc in unsteady flows (dashed curves — at $\theta = 0.1$, dash-dotted curves — at $\theta = 0.02$) in comparison with time-independent cavities (shown by solid curves) at the same values of σ (shown by numbers). For all cavities: $\sigma(0) = 0.136$. For unsteady cavities $\sigma(t) = \sigma(0)\gamma^2$, $a = -\theta$, $\gamma = (1 - \theta t^*)^{-1}$.

5. Problems for unsteady flows

Problems for inviscid flows with unsteady boundaries are more complex even without taking into account gravitation and capillary forces. For them the dynamic condition (4) on the cavity surface can be represented in the following form:

$$\frac{\partial\Phi}{\partial s} = \sqrt{1 + \sigma - 2\gamma\left(a\gamma\Phi + \frac{\partial\Phi}{\partial t^*}\right)}. \qquad (39)$$

Its right part depends on instantaneous values of three parameters: σ, $a = \frac{D}{U_\infty^2(0)}\frac{dU_\infty(t)}{dt}$ and $\gamma = \frac{U_\infty(0)}{U_\infty(t)}$; here $t^* = \frac{U_\infty(0)}{C}$. The unsteady analogue of equation (15)

$$\frac{qb}{2} - \frac{\partial(Uh)}{\partial l} - \frac{\gamma h}{t^{**}} = 0 \qquad (40)$$

contains t^{**} — difference of two successive dimensionless moments of time t_+^* and t_-^*; here l — tangent to the current line (which, as a rule, does not coincide with the free surface for unsteady flows). It must be noted that as opposed to the situation solved by equations (17), (20), (21), here variations of L are directly connected with the change in t, and not the σ. Therefore, the analogue of equation (21) for unsteady flows serves to determine t. Quasi-linearization of equation (4) with its right part described by equation (39), followed by the inversion of Cauchy integrals results in a cumbersome formula, which is omitted here.

Some calculated examples from [14] for unsteady flows are shown in Fig. 17. It can be seen that for the disc motion with a strong deceleration the analysis of time-independent flow results in a considerably underestimated cavity length. In this example at $\sigma = 0.5$ the result of time-independent theory is as low as 23% of the result of unsteady theory. The stability of free surface in examples from Fig. 17 was kept due to very high of $|a|$, although, as it is found in [61], boundaries of unsteady cavities in ideal fluids, in general, are unstable.

The most often observed cavitating flow is that with very low $|a|$, however, in reality it is unsteady too. For this type of unsteady flow it is difficult to achieve convergence of the iteration process similar to the convergence shown in

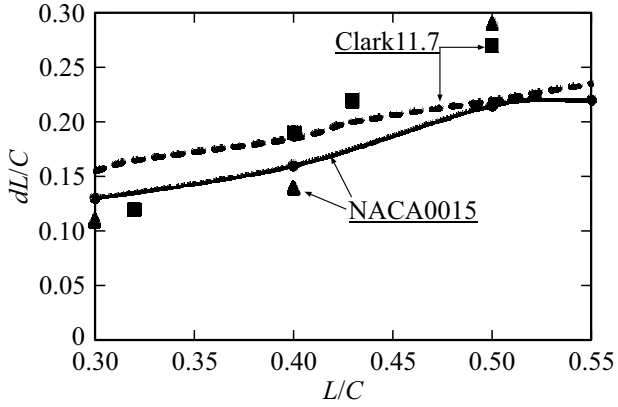

Figure 18. Comparison of the calculation of [16] with experimental data of [53] for Clark11.7 and [54] for NACA0015; numerical results are shown by lines.

Fig. 9. Due to this fact, the initial quasi-linear variant [7] of the Ivanov's method becomes preferable for them. Then solutions for the time-independent cavitation for a given σ using the Riabouchinsky's scheme can be considered as initial unperturbed solutions. This variant was used in [62] to calculate such cavities on blades and in [17] - on ClarkY-11.7 and NACA-0015 hydrofoils. As it is shown in Fig. 18, coincidence of calculated and measured [63,64] pulsation of cavity lengths dL is satisfactory, at least up to $L = 0.5C$.

The calculations presented in Fig. 18 took into account the elasticity of the hydrofoil and the compressibility of the cavity. These factors were taken into account in the right part of equation (2), but they did not have effect on the calculation scheme. However, it is necessary to note that statements of problems with free boundaries continue to be further defined [65], even for a fewer number of physical parameters.

Conclusion

Calculations of flows with free boundaries are a special class of non-linear boundary problems for differential equations, because boundaries of their definition domains are unknown and should be found. The described iteration method is based on quasi-linearization of the boundary conditions for potentials followed by solving of integral Fredholm equations of the second kind and singular integral equations in sequence at all iterations. Variants of these method are modifications (generalizations) of the method, developed by A.N. Ivanov.

The general formulation of the method and its modifications for specific types of flows are presented together with numerous computational examples for them. Fundamentally, the similar modifications allow solving problems, which are different from physical standpoint.

Conflict of interest

The author declares that he has no conflict of interest.

References

[1] G. Birkoff, E. Zarantello, *Sledy, strui i kaverny* (Nauka, M., 1964) (in Russian)
[2] D. Riabouchinsky. Proc. London Math. Soc., **19**, 206 (1919).
[3] C. Brennen. J. Fluid Mechanics, **37**, 671 (1969).
[4] M.I. Gurevich, *Teoriya struy idealnoy zhidkosti* (Fizmatgiz, M., 1961) (in Russian)
[5] J.A. Geurst. Int. Shipbuilding Progress, **6**, 369 (1959).
[6] G. Birkhoff. Mathematical Analysis of Cavitation. UITAM Symp. High-Speed Flows, Leningrad (1971)
[7] A.N. Ivanov, Mekhanika i mashinostroenie, Izvestiya AN SSSR, **6**, 118 (1962) (in Russian)
[8] A.N. Ivanov, Trudy TsNII Ak. AN Krylova, **219**, 70 (1965) (in Russian)
[9] M. Tulin. J. Ship Res., **7**, 16 (1964).
[10] K.V. Aleksandrov, MZhG Izvestiya AN SSSR, **4**, 140 (1976) (in Russian)
[11] E.L. Amromin, A.N. Ivanov, MZhG Izvestiya AN SSSR, **4**, 50 (1976) (in Russian)
[12] A.V. Vasiliev, Trudy TsNII A.N. Krylova, **4** (288), 8 (1997) (in Russian)
[13] K.V. Aleksandrov, A.V. Vasiliev, Gidrodinamika vysokikh skorostei, NTO A.N.Krylova, **3**, 31 (1983) (in Russian)
[14] E.L. Amromin, V.A. Bushkovsky, PMM, **49**, 787 (1985) (in Russian)
[15] E.L. Amromin. Ocean Eng., **54**, 46 (2012).
[16] E.L. Amromin. ASME J. Fluids Eng., **141**, 114501 (2019).
[17] E.L. Amromin. ASME J. Fluids Eng., **142**, 111203 (2020).
[18] J.S. Ulhman. J. Ship Res., **31**, 107 (1987).
[19] C. Pelone, A. Rowe. ASME J. Fluids Eng., **110**, 182 (1988).
[20] A. Rowe, O. Blottiaux. J. Ship Res., **37**, 39 (1993).
[21] K.E. Afanas'ev, S.V. Stukalov, PMTF, **40**, 27 (1999) (in Russian)
[22] A.N. Varghese, J.S. Ulhman, I.N. Kirschner. ASME J. Fluids Eng., **127**, 41 (2005).
[23] J-K. Choi, G.L. Chahine. 28th Symp. *Naval Hydrodynamics* (Pasadena, California, USA 2010)
[24] F. Salvatore, H. Streckwall, T. van Terwisga, 1st Int. Symp. *Marine Propulsors* (Trondheim, (Norway 2009)
[25] F. Stern, J. Yang, Z. Wang, H. Sadat-Hosseini, M. Mousaviraad, S. Bhushan, T. Xing. 29th Symp. *Naval Hydrodynamics* (Gothenburg, 2012)
[26] E.L. Amromin. ASME J. Fluids Eng., **140**, 011103 (2018).
[27] W. Du, S.A. Kinnas. 29th ISOPE Conf. (Honolulu, 2019)
[28] A.N. Ivanov, *Gidrodinamika razvitykh kavitatsionnykh techeniy* (Sudostroenie, L., 1980) (in Russian)
[29] Yu. Gorbachev, A. Butuzov, A.N. Ivanov, V. Kalyuzhny, A. Pavlenko. 5th Intern. Congress *Marine Technology* (Athens, 1990)
[30] Yu. Gorbachev, A. Buyanov, A. Sverchkov, Morskoy flot, **1**, 26 (2015) (in Russian).
[31] A.N. Tikhonov, A.A. Samarsky, *Uravneniya matematicheskoy fiziki* (Gostekhisdat, M., 1951), (in Russian)
[32] A.G. Terentiev, I.N. Kirschner, J.S. Uhlman. *The Hydrodynamics of Cavitating Flows* (Backbone Publishing Company, Fair Lawn, 2011)

[33] P.P. Zabreiko, A.I. Koshelev, M.A. Krasnoselsky, S.G. Mikhlin, L. S. Rakovshchik, V.Ya. Stetsenko, *Integral'nye uravneniya* (Nauka, M., 1968) (in Russian)
[34] P.J. Roache. ASME J. Fluids Eng., **114**, 4 (2002).
[35] E.L. Amromin, ZhTF, **37**, 209 (1992) (in Russian)
[36] V.H. Arakeri. J. Fluid Mech., **68**, 779 (1975).
[37] E.L. Amromin, A.N. Ivanov, DAN SSSR, **262**, 823 (1982) (in Russian)
[38] I.E. Idel'chik, *Spravochnik po gidravlicheskin soprotivleniyam* (Mashinostroenie, M., 1992) (in Russian)
[39] A.S. Ramamurthy, R. Balanchandar, H.S. Govinda Ram. ASME J. Fluids Eng., **113**, 278 (1991).
[40] G. Yin, M.C. Ong. Ocean Eng., **223**, 108647 (2021).
[41] O.K. Kwon, R. Pletcher. ASME J. Fluids Eng., **108**, 64 (1986).
[42] L.V. Gogish, G.Yu. Stepanov, *Otryvnyye i kavitatsionnyye techeniya* (Nauka, M., 1990) (in Russian)
[43] A.A. Butuzov, MZhG Izvestiya AN SSSR, **2**, 83 (1966) (in Russian)
[44] J. Kopriva, E.L. Amromin, R.E.A. Arndt. ASME J. Fluids Eng., **130**, 031301 (2008).
[45] E.L. Amromin, G. Karafiath, B. Metcalf. J. Ship Res., **55**, 196 (2011).
[46] E.L. Amromin, A.N. Ivanov, D. Yu. Sadovnikov, MZhG Izvestiya RAN, **4**, 125 (1994) (in Russian)
[47] D. Sadovnikov, G. Trincas. 22nd Symp, *Naval Hydrodynamics* (Washington, DC, 1998)
[48] M. Umeyama. Phil. Trans. R. Soc. A, **376**, 20170103 (2017).
[49] J.H. Michell. Phil. Magazine, **36**, 430 (1893).
[50] X. Zhong, S. Liao. J. Fluid Mech., **843**, 653 (2018).
[51] J.Y. Holyer. J. Fluid Mech., **93**, 433 (1979).
[52] A.M. Abdilghanie, P.J. Diamessis. Theor. Comp. Fluid Dyn., **26**, 205 (2012).
[53] G. Covles. *Internal Waves* (School for Marine Science & Techn., Umass- Dartmouth 2009)
[54] D.C. Tretheway, C.D. Meinhart. Phys. Fluids, **14**, L9 (2002).
[55] J. Ou, B. Perot, J.P. Rothstein. Phys. Fluids, **16**, 4635 (2004).
[56] O.P. Orlov, A.V. Sverchkov, Trudy TsNII A.N. Krylova, **383**, 43 (2018) (in Russian)
[57] J.W. Gose, K.B. Golovin, M. Boban, J.M. Barros, M.P. Schultz, M. Perlin, S.L. Ceccio. J. Ship Research, **64**, 1 (2020).
[58] A.V. Vasil'ev, *Razrabotka metodov rascheta ploskikh kavitatsionnykh techeniy i prognozirovanie kromochnoy kavitatsii naturnykh grebnykh vintov* (TsNII A.N. Krylova, 1997) (in Russian)
[59] E.L. Amromin, V.A. Bushkovsky, ZhTF, **42**, 1121 (1997) (in Russian).
[60] G.A. Shneerson, I.A. Vecherov, D.A. Degtev, O.S. Koltunov, S.I. Krivosheev, S.L. Shishigin. Tech. Phys., **53** (10), 1278 (2008). https://doi.org/10.1134/S1063784208100046
[61] A.N. Kuznetsov, O.V. Troepolskaya, Trudy seminara po kraevym zadacham, **22**, 139 (1985) (in Russian)
[62] E.L. Amromin, A.V. Vasil'ev, E.N. Syrkin, MZhG Izvestiya RAN, **28**, 57 (1993) (in Russian)
[63] G.Wang, Q. Wu, B. Huang. Acta Mech. Sin., **33**, 685 (2017).
[64] E.J. Chae, D.T. Akcabay, A. Lelong, J.A. Astolfi, Y.L. Young. Phys. Fluids, **28**, 075102 (2016).
[65] D.V. Maklakov, A.I. Lexina. J. Fluid Mech., **936**, A30 (2022).